

pubs.acs.org/JPCC Article

Nonlinear Hybrid Surface-Defect States in Defective Bi₂Se₃

Sharmila N. Shirodkar* and Pratibha Dev*



Cite This: J. Phys. Chem. C 2022, 126, 11833-11839



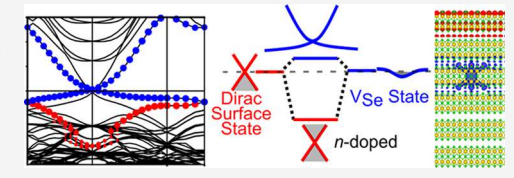
ACCESS I

Metrics & More

Article Recommendations

Supporting Information

ABSTRACT: The surface states of topological insulators are assumed to be robust against non-magnetic defects in the crystal. However, recent theoretical models and experiments indicate that even non-magnetic defects can perturb these states. Our first-principles calculations demonstrate that the presence of Se vacancies in Bi_2Se_3 , has a greater impact than a mere n-doping of the structure, which would just shift the Fermi level relative to the Dirac point. We observe the emergence of a nonlinear band pinned near the Fermi level, while the Dirac cone



splits and shifts deeper into the valence and conduction bands. We attribute these features in the band structure to the interaction between the surface and defect states, with the resulting hybridization between these states itself depending on the position and symmetry of the Se vacancy relative to the surfaces. Our results bring us a step closer to understanding the exotic physics emerging from defects in Bi_2Se_3 that remained unexplored in prior studies.

■ INTRODUCTION

Topological insulators are a new class of materials with a gapped bulk and metallic surfaces (for 3D materials) or edges (for 2D materials).^{1,2} These surface states are topologically non-trivial and originate from the strong spin-orbit coupling that preserves time-reversal symmetry. They are known to be robust against defects, strain, and disorder, assuming that the perturbation is modest enough to preserve the original character of the material. Since these surface states exhibit Dirac fermion behavior (linear dispersion), not only are they being explored for applications in quantum computing and spintronics, but their topological protection also allows one to test and explore exotic and fundamental concepts in physics, such as Majorana particles³ and magnetic monopoles. ⁴ As different proposed applications of topological insulators depend on the assumption of a linear Dirac cone, it is critical to understand if the surface states indeed remain unperturbed or if they are reshaped by the non-magnetic defects and to what extent. In fact, a recent theoretical model and experiment⁵⁻⁷ indicate that the latter is indeed the case. However, earlier first-principles calculations^{8,9} of these defects did not consider the reshaping of the surface states due to their interactions with defect states.

Among the bismuth selenide family of compounds (Bi_2Se_3 , Sb_2Te_3 and Bi_2Te_3), $Bi_2Se_3^{10,11}$ is the most widely studied 3D topological insulator, with a large bulk-band gap of 0.3 eV. Selenium vacancies (VSe) are known to be a common defect in Bi_2Se_3 and are assumed to be responsible for the n-type doping of the as-grown crystals. Due to the high volatility of selenium, the formation of additional vacancies on the surface of cleaved Bi_2Se_3 slabs is expected. This is possibly responsible for the observed aging of the slabs as they show changes in electronic properties with time. Though a vast literature exists on the formation energy of Se vacancies in Bi_2Se_3 , 8,9,17-19 very little is discussed about the nature of the defect states, their

placement in the electronic band structure, and the effect of their positions on the properties of $\mathrm{Bi}_2\mathrm{Se}_3$ surface states. Furthermore, most theoretical works have either considered very large densities of vacancies, such as a surface termination with all top selenium atoms removed, or symmetric defects on both surfaces that preserve the inversion symmetry of the slab. Hence, the effect(s) of lower concentrations of vacancies on $\mathrm{Bi}_2\mathrm{Se}_3$ remain unknown. To address these important questions, we carry out a detailed analysis on the effect of Se vacancies on the Dirac cone of the $\mathrm{Bi}_2\mathrm{Se}_3$ slabs and explore the coupling between the surface and defect bands as well as their emergent signature in the band structure and STM images.

COMPUTATIONAL DETAILS

The SIESTA (Spanish Initiative for Electronic Simulations with Thousands of Atoms) package 20,21 was used to carry out the density functional theoretical (DFT) calculations. A plane wave mesh cutoff of 300 Ry was used for non-spin polarized calculations, whereas a lower cutoff of 150 Ry was used for calculations including spin—orbit interactions. The electron—ion interactions were modeled with fully relativistic norm-conserving pseudopotentials obtained from PseudoDojo, 22,23 with exchange correlation energy between electrons approximated by the GGA functional parameterized by Perdew—Burke—Ernzerhof (PBE). 24 A double zeta-polarized basis set was used in our calculations. The Brillouin zone (BZ) integrations were carried out over a Monkhorst Pack k-point

Received: May 6, 2022 Revised: June 23, 2022 Published: July 8, 2022





mesh of size $6\times6\times6$ for the primitive bulk cell and $6\times6\times1$ for a slab of size $1\times1\times nQL$, where nQL stands for the number of quintuple layers (QL). Defects were created in supercell slabs of sizes $6\times6\times6$ QLs and $5\times5\times7$ QLs. Only BZ center integrations were carried out for the defective supercells.

The bulk primitive cell was relaxed (including spin-orbit coupling) until the Hellman-Feynman forces on the atoms were < 0.01 eV/Å and the stress components in each direction were $< 0.001 \text{ eV}/\text{ Å}^3$. This relaxed bulk structure was used to create $1\times1\times nQL$ (nQL = 6, 7) slabs, which was further relaxed (atoms only, with spin-orbit coupling) until the Hellman-Feynman forces on the atoms were < 0.01 eV/Å. This slab structure was then periodically repeated in the in-plane lattice directions to generate the 6×6×6 QLs (1080 atoms) and 5×5×7 QLs (875 atoms) supercell slabs. To estimate the structural relaxation due to Se vacancy defects, we carried out non-spinpolarized calculations on the defective supercell slabs, and the atoms were allowed to relax until the Hellman-Feynman forces on the atoms were < 0.04 eV/Å. Because we exclude the spinorbit effects in the relaxation calculations, we keep the Bi atoms fixed in their respective planes (allowed to move in-plane) since GGA parameterization overestimates the interplanar spacing (a known drawback). This constraint is reasonable since it mimics experimental slabs, where the defect concentration is approximately two orders of magnitude lower than in our calculations depending on the quality of the sample and would not affect the bulk interplanar spacing significantly. A vacuum of 24 Å was included in the non-periodic direction to minimize the interaction between the periodic images.

■ RESULTS AND DISCUSSION

Vacancy Configurations. Bulk Bi₂Se₃ has R3m (#166) space group symmetry with (a) Bi at Wyckoff position 6c (0,0,0.3985) and (b) Se with two symmetry inequivalent Wyckoff positions, 3a (0,0,0) and 6c (0,0,0.2115), and lattice constants a = b = 4.19 Å and c = 28.63 Å. ²⁵ It is a layered material with each layer containing five atoms (a formula unit) and therefore known as a quintuple layer (QL). The QLs have -A-B-C- stacking along the "z (c)" direction. The DFT estimates of lattice constants for the $1\times1\times nQL$ (nQL = 6 and 7) cell are a = b= 4.21 Å, i.e., overestimation by $\sim 0.4\%$ from the experimental value, whereas the estimated bulk lattice parameter, c = 28.92 Åis overestimated from the experimental value by 1%, well within the limits of DFT errors and therefore known as a quintuple layer (QL). Due to the difference between the electronic topology of the bulk with respect to the vacuum, cleaving the bulk into a slab gives rise to topologically protected Dirac surface states at the Fermi level assuming that the slab is thick enough to reduce interaction between the top and bottom surfaces. For slabs with $nQL \ge 6$, we find that the surface states become almost degenerate (i.e., produce a Dirac cone) at the Fermi level with a negligible gap between the conduction and valence band Dirac cones (< 1 meV). Pertsova et al. 26 have shown that this gap essentially goes to zero for > 40 QLs, which is when the top and bottom surface states become decoupled.

We construct $6\times6\times6$ QLs and $5\times5\times7$ QLs slabs to study the effects of Se vacancy defects on the surface states, with the two slabs representing different in-plane defect densities. In the $6\times6\times6$ QLs slabs, we create single VSe defects that break the inversion symmetry of the slab, capturing the defect- and substrate-induced asymmetry in experimental samples. On the other hand, in the $5\times5\times7$ QLs slabs, we create pairs of VSe defects that conserve the inversion symmetry of the top and the

bottom QL layers, allowing for a direct comparison with the existing literature. A comparison of results for the 6×6×6 QLs and 5×5×7 QLs slabs also allows us to highlight and differentiate between the effects of inversion symmetry breaking on the band structure and those due to defects themselves. As the overall results for the two structures are qualitatively similar, those for the 5×5×7 QLs slab are discussed in the Supporting Information. In both the 6×6×6 QLs and 5×5×7 QLs slabs, we create Se vacancies at the symmetry-inequivalent Wyckoff positions (3a and 6c) at the surface and in the interior (i.e., bulk) of the slab. Since the surface breaks the symmetry between the two Se atoms at 6c, we distinguish them as Se1 on the surface and Se1' below the surface (interface of topmost and next QL). Se2 is the Se atom at the 3a site, which is sandwiched between two BiSe layers (see Figure 1A). We will henceforth refer to

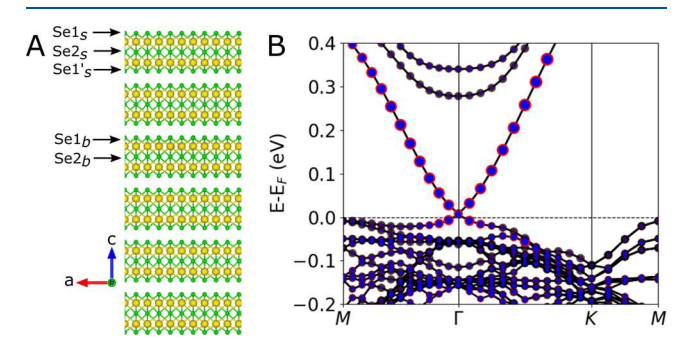


Figure 1. Structural model ($6\times6\times6$ QLs slab) and electronic structure of pristine Bi₂Se₃. (A) Symmetry inequivalent positions (Se1, Se1', and Se2) at which defects are created in the surface layer (subscript s) and in the bulk (subscript b). Note: the $6\times6\times6$ QLs slab is separated from its periodic image in the c-direction by 24 Å of vacuum. Se (Bi) atoms are shown by green (yellow) circles. (B) Electronic structure of pristine $6\times6\times6$ QLs slab, showing the Dirac cone emerging from the topological surface states at the Fermi level. The bands are colored to show contributions from different QLs to the electronic states (red = top QL, blue = bottom QL, and black = bulk contributions). The charge density plots of the wavefunctions are given in Figure S1.

vacancies in the surface (bulk) QL with a subscript "s" ("b"). An Se vacancy in a 6 ×6×6 QLs slab corresponds to a defect concentration of $\sim 10^{19}~\rm cm^{-3}$ (in-plane concentration = 2.6 × $10^{13}~\rm cm^{-2}$), comparable to the values reported in experiments, 17,28 which range from 10^{11} to $10^{20}~\rm cm^{-3}$. We note that previous theory works simulated a single Se vacancy per 3×3 in-plane supercell, while we use 6×6 and 5×5 in-plane supercells. The small supercell size in the earlier works results in stronger interactions between the periodic images of the vacancies, changing the effect of the defect states on the topological surface states of $\rm Bi_2Se_3$. The band structure of a pristine 6×6×6 QLs slab is shown in Figure 1B and shows the Dirac cone at the Fermi level.

Bulk Vacancies. We first explore how the vacancies in the bulk of the $\mathrm{Bi}_2\mathrm{Se}_3$ slab modify its electronic structure properties. The band structures for the two inequivalent defects, $\mathrm{VSe1}_b$ and $\mathrm{VSe2}_b$, are plotted in Figure 2A,C. The contributions of the top (bottom) surface (QL) to the electronic states are drawn with red (blue) circles; black circles represent the contribution of the bulk. Note that the states at the Γ and M points in the Brillouin zone (BZ) are doubly degenerate due to their topological nature. The defect breaks the structure inversion symmetry (SIA) of the slab, ²⁹ with the top QL being closer to the defect. This lifts the degeneracy of the surface states localized on the top and bottom

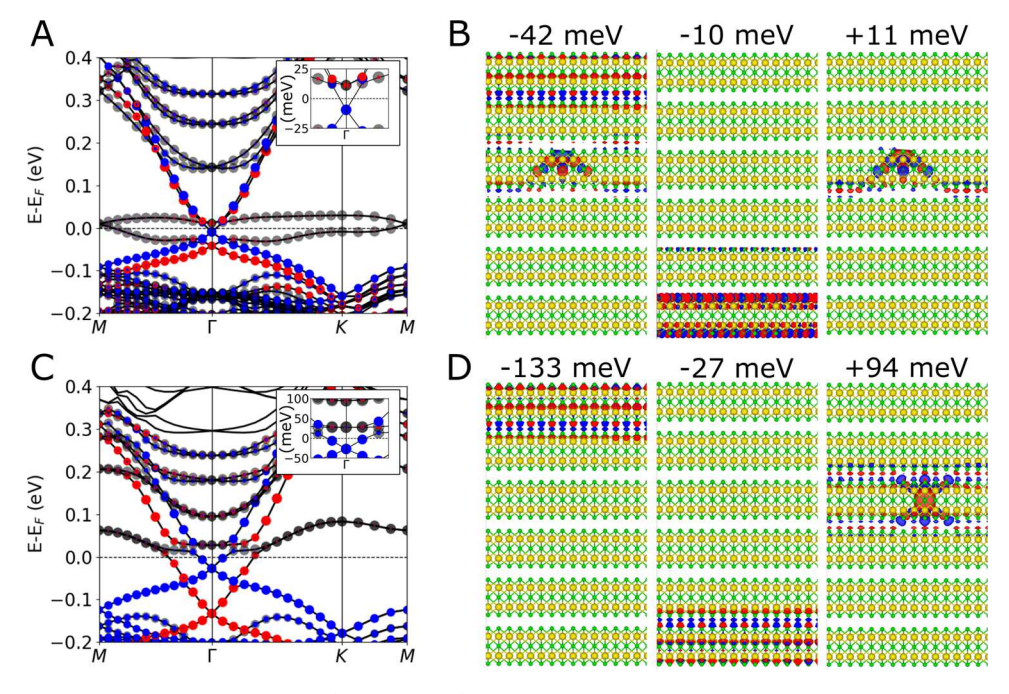


Figure 2. Electronic band structure and wavefunctions (at the Γ -point) of bulk Se vacancies in a 6×6×6 QLs slab. Band structures of (A) VSe1_b and C) VSe2_b are colored to show contributions from different QLs to the electronic states (red = top QL, blue = bottom QL, and black = bulk contributions). The insets are the zoomed-in band structures at the Fermi level and the Γ -point in the BZ. Note that the energy units in the insets are meV as opposed to eV in the main plot. The charge densities of the wavefunctions are shown in (B) for VSe1_b and D) VSe2_b. Se (Bi) atoms are shown by green (yellow) circles. The opposite phases of the wavefunctions that are calculated at the Γ -point are denoted by red and blue colors in the charge density plots.

surfaces, with the top surface state moving lower in energy due to its larger interaction with the defect. The Dirac cones associated with the top surface states are shifted by around -42 and -133 meV below the Fermi level for VSe1_b and VSe2_b, respectively. In contrast, for the VSe2_b in $5\times5\times7$ QLs slab (see Figure S2C), both the Dirac cones are degenerate due to conservation of inversion symmetry. The shift of the Dirac point below the Fermi level, which is due to interaction of the surface states with the defect high (discussed later in detail), likely depends on the distance of the defect from the surface and is expected to be reduced for defects that are much farther away from the surfaces in thicker slabs.

Figure 2B,D shows the wavefunctions at the Dirac points (i.e., Γ -point) for the two bulk defects. In the case of VSe1_b, we find that the topological character (linear dispersion) for the top and bottom surface states is preserved, with the associated Dirac cones shifted below the Fermi level by about -42 and -10 meV (see Figure 2B, leftmost and middle panels). Figure 2B (right panel) also shows the unoccupied conduction band minimum at Γ . It is about +11 meV above the Fermi level and is mostly localized around the defect site. Interestingly, the wavefunctions at about -42 meV and a lower isosurface plot of the state at about +11 meV show that they are actually admixtures of the top surface states and defect states, being bonding and anti-bonding states, respectively. In the case of the bulk defect, VSe2_b, the top surface state is shifted by around -133 meV, whereas the bottom surface state at around -27 meV is localized to the bottom-most QL. Unlike the hybridization between surface and defect states seen for VSe1_b, the defect state associated with VSe2_b is decoupled from the surface states (see Figure 2D at -133 and -27 meV). Anti-crossing of the surface states and the defect band (see Figure 2C at around +0.05 eV) confirms their decoupling. This shows that although the VSe2_b defect is at a similar distance from both the surfaces as VSe1_b, the Wyckoff position of the Se vacancy in bulk affects the electronic structure properties of a Bi_2Se_3 slab differently. In part, these differences might stem from the fact that a VSe2 defect preserves the intralayer inversion symmetry as opposed to VSe1, which breaks it. We find similar behavior in the $5\times5\times7$ QLs slab with VSe2_b (see Figure S3).

Surface Vacancies. Unlike bulk Se vacancies where the interaction between the defect and surface states can be reduced by considering thicker slabs, surface vacancies merely by virtue of their position are inherently coupled to the surface states. For the surface defects VSe1, VSe1, and VSe2, the calculated band structure clearly shows strong interactions with the topological surface states (see Figure 3A,C,E) and the emergence of a nonlinear (almost parabolic) band at the Fermi level (that was missing in for bulk vacancies). In addition, the top QL state shifts much deeper into the valence band as compared to that in the presence of bulk defects (see Figure S6 for the band structure plotted for the wider-energy range). Following the signatures of the top QL contribution to the band structure (colored red in Figure 3, left column) into the valence band, we identify these surface states by plotting the charge densities of their wavefunctions at Γ-point (see leftmost column in Figure 3B,D,F). The surface states of the defective top QL are shifted by around -225, -125, and -357 meV for VSe1, VSe1, and VSe2, respectively. Not only are they localized to the topmost QL, they also exhibit linear dispersion in the band structure (see Figure S6) with the same Dirac cone features as in a pristine slab (see Figure 1B). In each of these Dirac cones that are found much deeper in the valence band, the lower branch of the cone shows the expected upward dispersion, which arises from the k^5 term in the Dresselhaus spin-orbit coupling.³¹ This further confirms the topological protection of surface states in Bi₂Se₃ even in the presence of a considerably large in-plane concentration of Se vacancies at the surface.

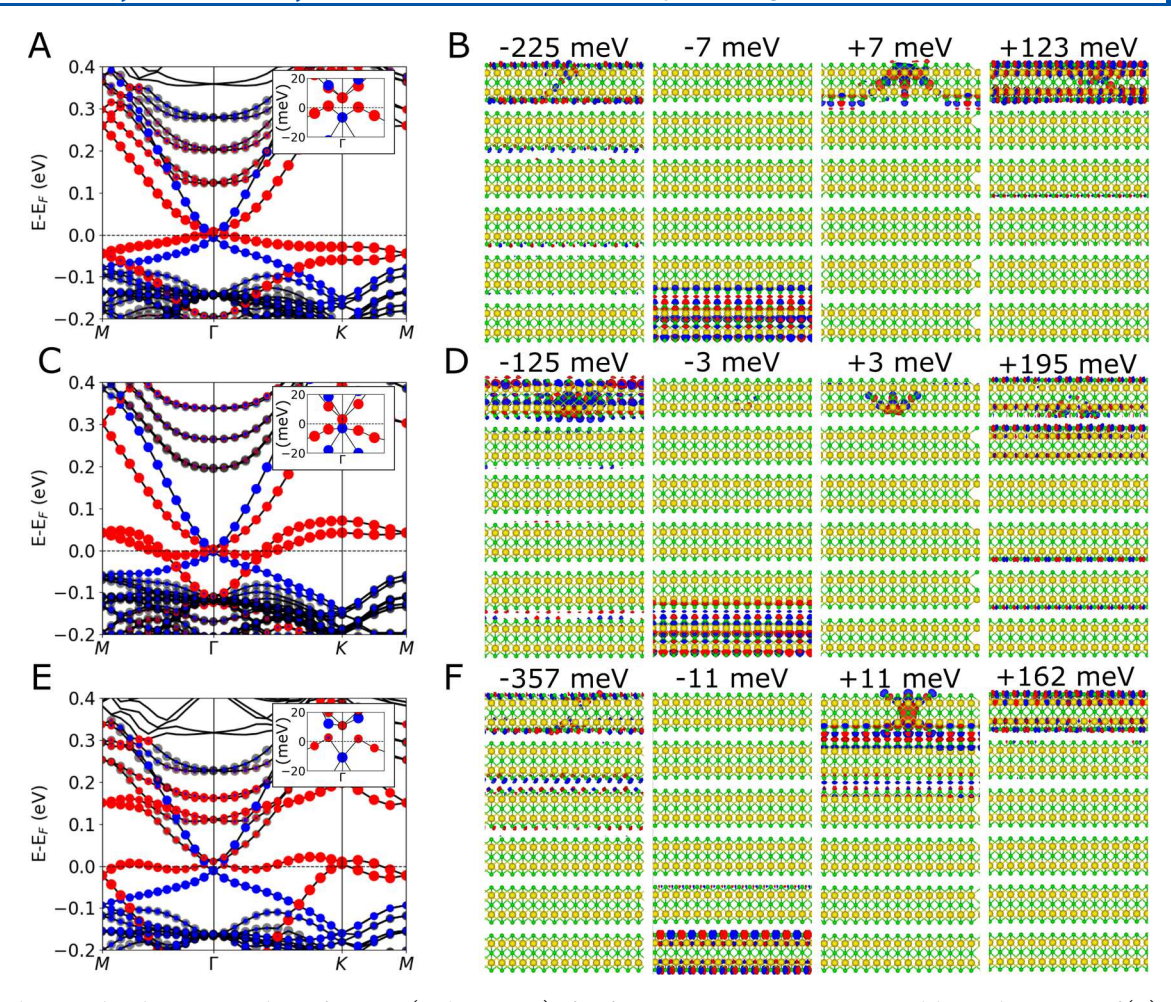


Figure 3. Electronic band structure and wavefunctions (at the Γ -point) of surface Se vacancies in a 6×6×6 QLs slab. Band structures of (A) VSe1 $_s$ (C) VSe1 $_s$, and (E) VSe2 $_s$ are colored to show contributions from different QLs to the electronic states (red = top QL, blue = bottom QL, and black = bulk contributions) The insets are the zoomed-in band structures at the Fermi level and the Γ -point in the BZ. Note that the energy units in the insets are in meV, as opposed to eV in the main plot. The charge densities of the wavefunctions are shown in (B) for VSe1 $_s$ (D) for VSe1 $_s$, and (F) for VSe2 $_s$. Se (Bi) atoms are shown by green (yellow) circles. The opposite phases of the wavefunctions that are calculated at the Γ -point are denoted by red and blue colors in the charge density plots.

Furthermore, we see a shift of the Dirac cone from the bottom (pristine) layer (see Figure 3, band structure in blue and second panel of the wavefunctions) below the Fermi level by -7, -3, and -11 meV for VSe1_s, VSe1_s, and VSe2_s, respectively. The downward shift from the Fermi level is a result of the intersurface coupling between the defect and bottom QL.²⁹ This is confirmed from the smaller shift of -5 meV for a single surface vacancy in the 5×5×7 QLs slab (see Figure S5) and an equal and opposite shift seen in the hybrid, mostly defect-type, state around the Γ -point (Figure 3 B,D,F, third panel). We expect the shift to reduce with increasing slab thickness. Interestingly, we also find that the top part of the surface state cone from the top QL surface has shifted into the conduction band by around 123 and 162 meV for VSe1_s and VSe2_s, respectively (Figure 3B,D,F, rightmost panel). On the other hand, the surface state at \sim 195 meV for VSe1, shows greater delocalization, with significant contributions from the next QL due to hybridization with the bulk conduction band states. The splitting of the top and bottom part of the surface state Dirac cone agrees with the work of Black-Schraffer et al.³²

Origin of the Defect Band. In addition to identifying the Dirac points associated with the top and bottom surface states, we investigate the origin of bands lying between -0.2 and 0.2 eV

(see Figure 3A,C,E), focusing on the nonlinear bands near the Fermi level in this range. Figure 4A is a schematic diagram depicting our proposed origin of these bands. The Se vacancy within the top QL introduces SIA, 29 which lifts the degeneracy between the top (dashed yellow in Figure 4A) and bottom QL layer (solid purple) Dirac cones. The Se1 and Se1' positions possess 3m point group symmetry, whereas the Se2 position has -3m symmetry. Here, we focus our discussion on the VSe1, defect, but a similar explanation is valid for VSe2, and VSe1, as well. Due to the 3*m* symmetry of the VSe1s defect, the dangling "p" orbitals of the Bi atoms (near the vacancy) split as the singly degenerate A1 and doubly degenerate E bands. The A1 defect band is near the Fermi level, whereas the E bands are higher in the conduction band at ~ 0.8 eV (see Figure S9). On closer inspection of the conduction bands (see Figure 3A,C,E), we find states in the bulk band gap that were absent for the pristine slab (see Figure 1B). These states are the quantum well (QW) states that are induced by the band bending at vacuum and defective QL interface due to the symmetry breaking and doping of the top QL by the defect.²⁷

In the absence of any interaction between the defect and the surface states, the band structure would resemble Figure 4A (lower branch, middle plot). Interaction between the defect/

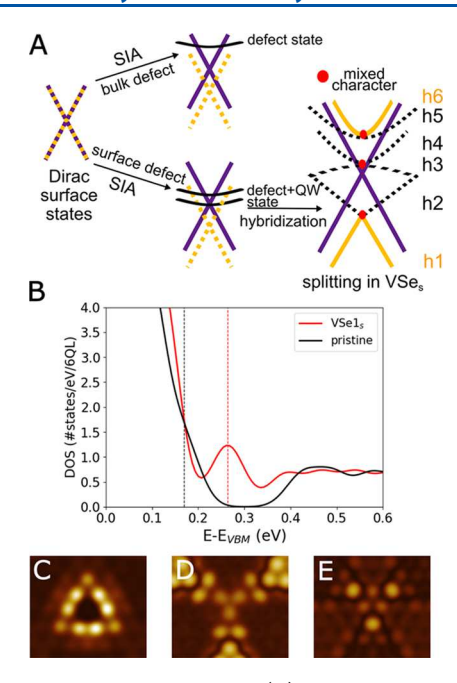


Figure 4. Defect band and its origin. (A) Energy diagram postulating the origin of hybrid bands (h1–h4) due to interaction between Se vacancies and surface states. SIA stands for structural inversion asymmetry. The defect and quantum well (QW) states are shown in black, and the top and bottom QL Dirac cones are shown by yellow dashed and purple solid lines, respectively. (B) Comparison of the density of states (DOS) of the pristine 6 QLs Bi_2Se_3 slab (black) and $VSe1_s$ (red). The Fermi levels are marked by black (pristine) and red (defect) dashed lines. Constant-height STM images of (C) $VSe1_s$, (D) $VSe1_s'$, and E) $VSe2_s$ for V = +0.3 V (sampling the conduction band). $VSe3_s$ can be distinguished by a dark spot in its STM image, $VSe3_s'$ is distinguishable by a pattern resembling the nuclear radiation symbol, and $VSe3_s$ can be distinguished by three bright spots.

QW and topologically protected top surface states^{32,33} creates hybrid bands (h1-h6), shown in Figure 4A, lower branch, rightmost plot (also see the Supporting Information S7 for a numerical model based on ref 33). Here, the defect band spinsplits into two branches, one of which mixes with the lower part of the Dirac cone of the top QL. The Dirac cone that is deep in the valence band is a hybrid (h1+h2) with the lower part (h1) originating from the top QL surface state and the upper part (h2) from the defect. This mixing is evident in the charge densities of the wavefunctions (see Figure 3B,D,F at the Γ point). h3 is the other spin-split defect band that primarily interacts with the lower part of the Dirac cone. Since the defect forms an integral part of the surface, h1, h2, and h3 also acquire some defect and surface characters, respectively. Similarly, the upper part of the original Dirac cone (of the top QL) mixes with the QW state²⁷ present above the Fermi level in the bulk gap region and forms, h4, h5, and h6 bands. Here, the nonlinear/ parabolic band (h4) above the Fermi level is mostly defect-like in character (see Figure S10). This mixing behavior observed here is quite different from an earlier work by Seixas et al.³³ where a "twinning" of the Dirac cone at the interface of a topological insulator and a trivial insulator was reported. In that case, the mixed states only emerge at the high-symmetry points in the BZ. Hence, the hybridization, which results in the nonlinear/parabolic band, h4, described in our work, is a unique signature characterizing the Se vacancies in Bi₂Se₃. h1-h6 also exhibit a helical spin-texture (see Figure S11), being admixtures of the topologically protected surface states and defect states.

Lastly, we note the interaction between the defect and the bottom QL. This shifts the defect state and the bottom surface state above and below the Fermi level, respectively. The magnitude of the shift appears to be correlated to (a) how deep the h1+h2 band has shifted into the valence band and (b) the screening of the vacancy by the adjacent layers. The shift is larger for VSe2, in comparison with VSe1, and VSe1, as the h1+h2 hybrid band is also lower (see Figure 3 A,C,E). In the case of VSe1, though it has similar placement in the QL as VSe1, the screening effect of the adjacent QL for the VSe1, makes the splitting negligibly small (see Figure S12). A quantitative analysis of the extent of the defect and surface state splitting (h1, h6 and h3, h4 separation) has been explored in a generalized theoretical model of a strong three-dimensional topological insulator by Black-Schraffer et al.,³² where they show that the magnitude of the shift of the surface states into the conduction and valence bands is dependent on the strength of the defect

The h1-h6 bands preserve the topological character of the surface states, i.e., they span the bulk energy gap and connect the bulk valence and conduction bands. They are similar to the socalled "topological dangling bond states", 8,34 which were reported when an entire layer of Se atoms is missing from the top QL. It is important to note that the presence of surface states (h1 and h6) outside the bulk band gap region encourages scattering from the bulk states. Thus, the surface states lose their protection from spin-backscattering processes. The dispersion of h2 and h3 for VSe1, and VSe2, (between energies of -0.05 and 0.05 eV; Figure 3C,E), gives rise to multiple Fermi-surface nestings, which is similar to Bi₂Se₃ slabs cleaved along different planes.³⁴ This feature allows spin-backscattering processes previously forbidden in a pristine slab. For lenergies $l \ge 0.05$ eV, the multiple Fermi-surface nesting disappears and the spinbackscattering processes again become forbidden. Thus, by controlling the position of the Fermi level via gating, one can control the surface spin current in defective Bi₂Se₃. This possibility opens up new applications in spintronics that can replace existing semiconductor-based devices.

It is important to note that even though the parabolic band, h4 (see Figure 3 A,C,E), looks like a 2DEG (2D electron gas) 15,16 in Bi $_2$ Se $_3$, its origin and spin texture reveal the opposite. h4 shows spin-momentum locking with a slight out-of-plane "z" component (due to defects; 35 see Figure S11), in contrast with a 2DEG, which is spin-degenerate. 15,16 A 2DEG band in the topological insulators is known to originate from band bending induced by defects 36 or by changes in the van der Waals gap between layers, 37 not hybridization. It is also formed well above the Dirac point 15,16,36,37 in the conduction band. These differences lead us to believe that h4 is a previously unreported characteristic of Se vacancies in Bi $_2$ Se $_3$. The signature of the defect is also seen as a resonant defect state above the Fermi level in the density of states (see Figure 4B), consistent with predictions and observations $^{5-7,30}$ in earlier works.

Our calculations for defect in the 6×6×6 QLs also confirm experimental reports of a Rashba-like splitting of the conduction band states¹⁵ (see Figures 2 and 3 and the Supporting Information Figure S13). This splitting is due to inversion asymmetry introduced by the asymmetric defects in 6×6×6 QLs slabs, which is absent in the symmetrically placed defects in 5×5×7 QLs slabs (see Figure S2). The exception is the VSe1_s' defect, where this splitting is negligible. Although an exact explanation of the latter is outside the scope of this work, different contributing factors might include a countering of the

Rashba-like splitting by the effects of local strain (due to the defect) on the band structure or the screening of the defect potential (see Figure S12).

Figure 4C–E shows simulated STM images (at constant height and V = +0.3 eV) for surface defects, providing their experimental signatures. We find that our STM images are in reasonable agreement with experimental observations of Dai et al. Any difference could be due to sampling of a different energy range in our calculations.

CONCLUSIONS

Our detailed study of Se vacancies in Bi₂Se₃ shows that a neutral Se vacancy state hybridizes with the bottom part of the surface state Dirac cone and shifts it deeper into the valence band, i.e., it n-dopes the layer. On the other hand, the top part of the Dirac cone also hybridizes with the quantum well (bulk) state. The QW-defect-surface state interaction, in turn, gives rise to a nonlinear (parabolic) band with a primary defect character at the Fermi level while shifting the top Dirac cone into the conduction band. We find that the nonlinear bands at the Fermi level originating at the surface prohibit spin-backscattering processes for VSe1, just like the surface states in pristine Bi₂Se₃ slabs. Hence, in this structure, the directionality of the spin current at the surface is preserved. The origin, spin texture, and position with respect to the Fermi level of this band is unlike the 2DEG observed in Bi₂Se₃, ^{15,16} which makes it a unique feature of surface vacancies in this material. For the first time, our DFT results confirm the presence of such a defect band consistent with earlier reports. 5,6 The unique dispersion of this band allows one to switch the spin-backscattering processes "on/off" by controlling its occupancy, providing additional tunability to the spin current. Deterministic placement of Se vacancies can provide an added functionality to topological-insulator based applications in spintronics. This would be a considerable improvement over traditional semiconductor spintronic materials. Studying these defects under stress, strain, electric fields, and gas contaminants would be an exciting future scope of this work.

ASSOCIATED CONTENT

Supporting Information

The Supporting Information is available free of charge at https://pubs.acs.org/doi/10.1021/acs.jpcc.2c03142.

Results for symmetric Se vacancies in the 5×5×7 QLs slab, numerical model to explain the hybridization of defect states with the topological surface states, Rashba splitting in the electronic structure, spin-momentum locking plots, and convergence studies of the electronic structure with plane wave cutoff, displacement of Bi atoms, and Hamiltonian matrix elements (PDF)

AUTHOR INFORMATION

Corresponding Authors

Sharmila N. Shirodkar — Department of Physics and Astronomy, Howard University, Washington D.C. 20059, United States; Occid.org/0000-0002-9040-5858; Email: sharmila.shirodkar@howard.edu

Pratibha Dev — Department of Physics and Astronomy, Howard University, Washington D.C. 20059, United States; Email: pratibha.dev@howard.edu

Complete contact information is available at: https://pubs.acs.org/10.1021/acs.jpcc.2c03142

Notes

The authors declare no competing financial interest.

ACKNOWLEDGMENTS

We would like to thank Dr. Ivan Naumov for helpful discussions and inputs, and Dr. J. R. Knab for help with copy editing. This work was supported by W. M. Keck Research Foundation grant and NSF grant number DMR-1752840. We acknowledge the computational support provided by the Extreme Science and Engineering Discovery Environment (XSEDE) under project PHY180014, which is supported by National Science Foundation grant number ACI-1548562, and the Maryland Advanced Research Computing Center.

REFERENCES

- (1) Kane, C. L.; Mele, E. J. Quantum Spin Hall Effect in Graphene. *Phys. Rev. Lett.* **2005**, *95*, 226801.
- (2) Bernevig, B. A.; Hughes, T. L.; Zhang, S.-C. Quantum Spin Hall Effect and Topological Phase Transition in HgTe Quantum Wells. *Science* **2006**, 314, 1757–1761.
- (3) Grover, T.; Sheng, D. N.; Vishwanath, A. Emergent Space-Time Supersymmetry at the Boundary of a Topological Phase. *Science* **2014**, 344, 280–283.
- (4) Qi, X.-L.; Li, R.; Zang, J.; Zhang, S.-C. Inducing a Magnetic Monopole with Topological Surface States. *Science* **2009**, 323, 1184–1187
- (5) Miao, L.; Xu, Y.; Zhang, W.; Older, D.; Breitweiser, S. A.; Kotta, E.; He, H.; Suzuki, T.; Denlinger, J. D.; Biswas, R. R.; et al. Observation of a topological insulator Dirac cone reshaped by non-magnetic impurity resonance. *npj Quantum Mater.* **2018**, *3*, 29.
- (6) Zhong, M.; Li, S.; Duan, H.-J.; Hu, L.-B.; Yang, M.; Wang, R.-Q. Effect of impurity resonant states on optical and thermoelectric properties on the surface of a topological insulator. *Sci. Rep.* **2017**, *7*, 3971.
- (7) Teague, M. L.; Chu, H.; Xiu, F.-X.; He, L.; Wang, K.-L.; Yeh, N.-C. Observation of Fermi-energy dependent unitary impurity resonances in a strong topological insulator Bi2Se3 with scanning tunneling spectroscopy. *Solid State Commun.* **2012**, *152*, 747–751.
- (8) Yan, B.; Zhang, D.; Felser, C. Topological surface states of Bi2Se3 coexisting with Se vacancies. *Phys. Status Solidi RRL* **2013**, *7*, 148–150.
- (9) Wang, S.; Zhang, P. Native point defects in Bi2Se3: A first-principles study. *Phys. Lett. A* **2020**, 384, 126281.
- (10) Xia, Y.; Qian, D.; Hsieh, D.; Wray, L.; Pal, A.; Lin, H.; Bansil, A.; Grauer, D.; Hor, Y. S.; Cava, R. J.; et al. Observation of a large-gap topological-insulator class with a single Dirac cone on the surface. *Nat. Phys.* **2009**, *5*, 398–402.
- (11) Zhang, H.; Liu, C.-X.; Qi, X.-L.; Dai, X.; Fang, Z.; Zhang, S.-C. Topological insulators in Bi2Se3, Bi2Te3 and Sb2Te3 with a single Dirac cone on the surface. *Nat. Phys.* **2009**, *5*, 438–442.
- (12) Navrátil, J.; Horák, J.; Plecháček, T.; Kamba, S.; Lošťák, P.; Dyck, J. S.; Chen, W.; Uher, C. Conduction band splitting and transport properties of Bi2Se3. *J. Solid State Chem.* **2004**, *177*, 1704–1712.
- (13) Jafarpisheh, S.; Ju, A.; Janßen, K.; Taniguchi, T.; Watanabe, K.; Stampfer, C.; Beschoten, B. Reducing the Impact of Bulk Doping on Transport Properties of Bi-Based 3D Topological Insulators. *Phys. Status Solidi B* **2021**, 258, 2000021.
- (14) Kim, J.; Shin, E.-H.; Sharma, M. K.; Ihm, K.; Dugerjav, O.; Hwang, C.; Lee, H.; Ko, K.-T.; Park, J.-H.; Kim, M.; et al. Observation of Restored Topological Surface States in Magnetically Doped Topological Insulator. *Sci. Rep.* **2019**, *9*, 1331.
- (15) King, P. D. C.; Hatch, R. C.; Bianchi, M.; Ovsyannikov, R.; Lupulescu, C.; Landolt, G.; Slomski, B.; Dil, J. H.; Guan, D.; Mi, J. L.; et al. Large Tunable Rashba Spin Splitting of a Two-Dimensional Electron Gas in Bi₂Se₃. *Phys. Rev. Lett.* **2011**, *107*, No. 096802.
- (16) Bianchi, M.; Guan, D.; Bao, S.; Mi, J.; Iversen, B. B.; King, P. D. C.; Hofmann, P. Coexistence of the topological state and a two-

- dimensional electron gas on the surface of Bi2Se3. *Nat. Commun.* **2010**, 1, 128.
- (17) Stephen, G. M.; Naumov, I.; Tyagi, S.; Vail, O. A.; DeMell, J. E.; Dreyer, M.; Butera, R. E.; Hanbicki, A. T.; Taylor, P. J.; Mayergoyz, I.; et al. Effect of Sn Doping on Surface States of Bi2Se3 Thin Films. *J. Phys. Chem. C* **2020**, 124, 27082–27088.
- (18) West, D.; Sun, Y. Y.; Wang, H.; Bang, J.; Zhang, S. B. Native defects in second-generation topological insulators: Effect of spin-orbit interaction on Bi₂Se₃. *Phys. Rev. B* **2012**, *86*, 121201.
- (19) Dai, J.; West, D.; Wang, X.; Wang, Y.; Kwok, D.; Cheong, S.-W.; Zhang, S. B.; Wu, W. Toward the Intrinsic Limit of the Topological Insulator Bi₂Se₃. *Phys. Rev. Lett.* **2016**, *117*, 106401.
- (20) Soler, J. M.; Artacho, E.; Gale, J. D.; García, A.; Junquera, J.; Ordejón, P.; Sánchez-Portal, D. The SIESTA method forab initioorder-Nmaterials simulation. *J. Phys.: Condens. Matter* **2002**, *14*, 2745–2779.
- (21) Cuadrado, R.; Cerdá, J. I. Fully relativistic pseudopotential formalism under an atomic orbital basis: spin—orbit splittings and magnetic anisotropies. *J. Phys.: Condens. Matter* **2012**, *24*, No. 086005.
- (22) van Setten, M. J.; Giantomassi, M.; Bousquet, E.; Verstraete, M. J.; Hamann, D. R.; Gonze, X.; Rignanese, G.-M. The PseudoDojo: Training and grading a 85 element optimized norm-conserving pseudopotential table. *Comput. Phys. Commun.* **2018**, 226, 39–54.
- (23) García, A.; Verstraete, M. J.; Pouillon, Y.; Junquera, J. The psml format and library for norm-conserving pseudopotential data curation and interoperability. *Comput. Phys. Commun.* **2018**, 227, 51–71.
- (24) Perdew, J. P.; Burke, K.; Ernzerhof, M. Generalized gradient approximation made simple. *Phys. Rev. Lett.* **1996**, 77, 3865.
- (25) Nakajima, S. The crystal structure of Bi2Te3-xSex. J. Phys. Chem. Solids 1963, 24, 479–485.
- (26) Pertsova, A.; Canali, C. M. Probing the wavefunction of the surface states in Bi2Se3topological insulator: a realistic tight-binding approach. *New J. Phys.* **2014**, *16*, No. 063022.
- (27) Park, K.; Beule, C. D.; Partoens, B. The ageing effect in topological insulators: evolution of the surface electronic structure of Bi2Se3upon K adsorption. *New J. Phys.* **2013**, *15*, 113031.
- (28) Walsh, L. A.; Green, A. J.; Addou, R.; Nolting, W.; Cormier, C. R.; Barton, A. T.; Mowll, T. R.; Yue, R.; Lu, N.; Kim, J.; et al. Fermi Level Manipulation through Native Doping in the Topological Insulator Bi2Se3. ACS Nano 2018, 12, 6310–6318 PMID: 29874037,
- (29) Shan, W.-Y.; Lu, H.-Z.; Shen, S.-Q. Effective continuous model for surface states and thin films of three-dimensional topological insulators. *New J. Phys.* **2010**, *12*, No. 043048.
- (30) Xu, Y.; Chiu, J.; Miao, L.; He, H.; Alpichshev, Z.; Kapitulnik, A.; Biswas, R. R.; Wray, L. A. Disorder enabled band structure engineering of a topological insulator surface. *Nat. Commun.* **2017**, *8*, 14081.
- (31) Basak, S.; Lin, H.; Wray, L. A.; Xu, S.-Y.; Fu, L.; Hasan, M. Z.; Bansil, A. Spin texture on the warped Dirac-cone surface states in topological insulators. *Phys. Rev. B* **2011**, *84*, 121401.
- (32) Black-Schaffer, A. M.; Balatsky, A. V. Strong potential impurities on the surface of a topological insulator. *Phys. Rev. B* **2012**, *85*, 121103.
- (33) Seixas, L.; West, D.; Fazzio, A.; Zhang, S. B. Vertical twinning of the Dirac cone at the interface between topological insulators and semiconductors. *Nat. Commun.* **2015**, *6*, 7630.
- (34) Lin, H.; Das, T.; Okada, Y.; Boyer, M. C.; Wise, W. D.; Tomasik, M.; Zhen, B.; Hudson, E. W.; Zhou, W.; Madhavan, V.; et al. Topological Dangling Bonds with Large Spin Splitting and Enhanced Spin Polarization on the Surfaces of Bi2Se3. *Nano Lett.* **2013**, *13*, 1915—1919. PMID: 23614400,
- (35) Jin, K.-H.; Jhi, S.-H. Effect of atomic impurities on the helical surface states of the topological insulator Bi2Te3. *J. Phys.: Condens. Matter* **2012**, *24*, 175001.
- (36) Hsieh, D.; Qian, D.; Wray, L.; Xia, Y.; Hor, Y. S.; Cava, R. J.; Hasan, M. Z. A topological Dirac insulator in a quantum spin Hall phase. *Nature* **2008**, *452*, 970–974.
- (37) Menshchikova, T. V.; Eremeev, S. V.; Chulkov, E. V. On the origin of two-dimensional electron gas states at the surface of topological insulators. *JETP Lett.* **2011**, 94, 106.